Chapter 7

LONGITUDINAL MICROWAVE INSTABILITY FOR ELECTRONS

7.1 Bunch Modes

In the previous chapter, microwave instability for a coasting beam was discussed. The theory can also be extended to a bunch provided that two criteria are satisfied: (1) the bunch is much longer than the wavelength of the perturbation and (2) the growth time is much shorter than a synchrotron oscillation period. These criteria are mostly satisfied by proton bunches, but not by electron bunches. Another theory of longitudinal instability is therefore necessary for electron bunches.

For electron bunches, the synchrotron period is usually much shorter than the collective instability growth times. Thus, synchrotron oscillation cannot be neglected in the study of longitudinal instability. The revolution harmonics can no longer be studied individually; they are no longer good eigennumbers. Here, we must study the different modes of oscillation inside a bunch.

Because the beam particles execute synchrotron oscillations, it is more convenient to use instead circular coordinates r, ϕ in the longitudinal phase space. We define the coordinates of a beam particle by

$$\begin{cases} \tau \ = r\cos\phi \ , \\ p_\tau = r\sin\phi = \dfrac{\eta\delta}{\omega_s} \ , \end{cases} \tag{7.1}$$

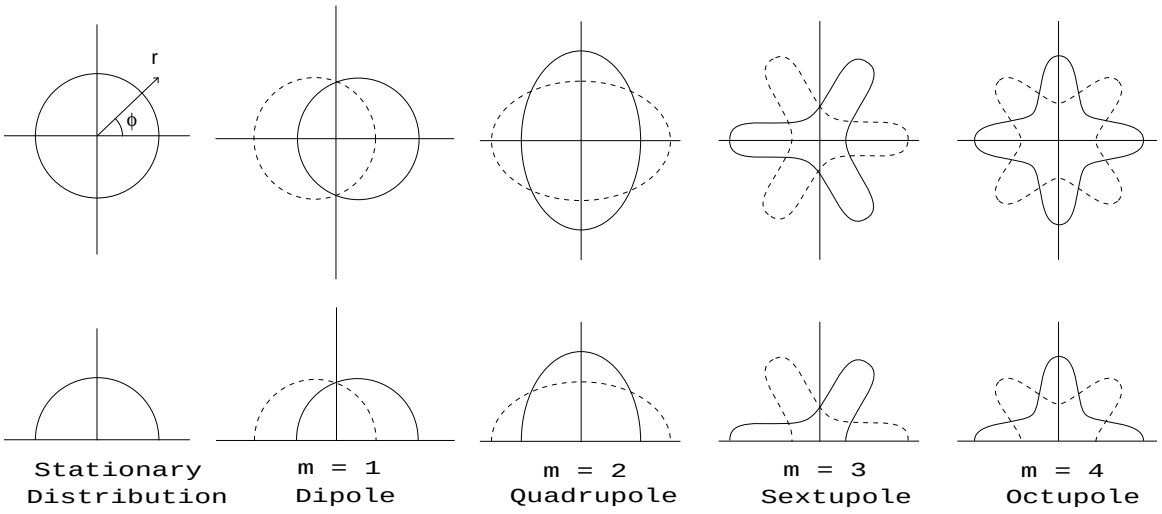

Figure 7.1: Azimuthal synchrotron modes of a bunch in the longitudinal phase space (top) and as linear density (bottom).

where τ is the time advance ahead of the synchronous particle and p_τ the conjugate momentum. A few azimuthal modes are shown in Fig. 7.1. One type of oscillation is azimuthal in ϕ, such as $\cos m\phi$. For example, $m = 1$ corresponds to a rigid dipole oscillation which we usually observe when the bunch is injected with a phase error. $m = 2$ corresponds to a quadrupole oscillation when there is a mismatch between the bunch and the rf bucket so that the oscillation appears to be twice as fast. The drawings show the motion of the bunch with the mth azimuthal mode. To obtain the mth azimuthal mode, the stationary distribution must be subtracted. For example, for the $m = 1$ mode with infinitesimal amplitude, after subtracting the stationary distribution we obtain a ring with positive charges on the right and negative charges on the left. The best description will be $\cos\phi$, and there are two nodes at $\phi = \pm\frac{\pi}{2}$. The $m = 2$ mode assumes the shape of $\cos 2\phi$ with 4 nodes at $\phi = \pm\frac{\pi}{4}$ and $\pm\frac{3\pi}{4}$. For the mth mode, the shape is $\cos m\phi$ with $2m$ nodes.

It is clear that to drive the higher azimuthal modes, *longitudinal impedance* of higher frequencies will be required. These modes can be understood mathematically if we follow a particle and record its time of arrival at a fixed location along the accelerator ring turn after turn. First assume a point particle. The signal recorded is

$$\text{signal} \propto \sum_{k=-\infty}^{\infty} \delta\left[s - kC_0 - v\hat{\tau}\cos\left(\frac{\omega_s s}{v} + \varphi\right)\right] \ , \tag{7.2}$$

where ω_s is the angular synchrotron frequency, C_0 is the length of closed orbit of the synchronous particle whose velocity is v. For the particle under study, the turn number is denoted by k, the amplitude of synchrotron oscillation or the maximum time arrival ahead of the synchronous particle is $\hat{\tau}$, and the initial synchrotron phase is represented by φ. It is safe to substitute $s = kC_0$ inside the argument of cosine because the amplitude of synchrotron oscillation is very much smaller than the circumference of the ring. We get

$$\begin{aligned} \text{signal} \;&\propto \int_{-\infty}^{\infty} \frac{d\omega}{2\pi v} \sum_{k=-\infty}^{\infty} e^{-i[s-kC_0-\hat{\tau} v \cos(k\omega_s C_0/v+\varphi)]\omega/v} \\ &= \int_{-\infty}^{\infty} \frac{d\omega}{2\pi v} \sum_{k=-\infty}^{\infty} \sum_{m=-\infty}^{\infty} i^m J_m(\omega\hat{\tau}) e^{-i(s-kC_0)\omega/v} e^{-im(k\omega_s C_0/v+\varphi)} \;, \end{aligned} \tag{7.3}$$

where the mathematic formula for Bessel function,

$$e^{ix\cos\phi} = \sum_{m=-\infty}^{\infty} i^m J_m(x)\, e^{-im\phi} \tag{7.4}$$

has been used. The summation over k can be performed using the Poisson formula,

$$\frac{1}{2\pi} \sum_{k=-\infty}^{\infty} e^{ik\theta} = \sum_{p=-\infty}^{\infty} \delta(\theta - 2\pi p) \;, \tag{7.5}$$

to obtain

$$\text{signal} \propto \int_{-\infty}^{\infty} \frac{d\omega}{C_0} \sum_{p=-\infty}^{\infty} \sum_{m=-\infty}^{\infty} i^m J_m\left[(p\omega_0 + m\omega_s)\hat{\tau}\right]\, \delta(\omega - p\omega_0 - m\omega_s)\, e^{-im\varphi} e^{-im\omega s/v}, \tag{7.6}$$

where $\omega_0/(2\pi) = v/C_0$ is the revolution frequency of the synchronous particle. Now we see all the azimuthal modes as sidebands of each harmonic line. The Bessel functions in the summation determines the amplitude of the sidebands. The synchrotron amplitude $\hat{\tau}$ is usually very much smaller than the revolution period. In this case, the lowest sideband $m = 1$ dominates. The revolution harmonics ($m = 0$) have roughly the same amplitude under the envelope of J_0 while the amplitudes of the $m = 1$ sidebands increase linearly with frequency under the envelope of J_1. If $\hat{\tau}$ is getting larger, however, the higher order sidebands ($m > 1$) will be observed. The $m = 2$ sidebands can have larger amplitudes than the revolution harmonics ($m = 0$) and the $m = 1$ sidebands when J_2 assumes a maximum. This is illustrated in Fig. 7.2, where, for simplicity, only the positive frequency part has been shown.

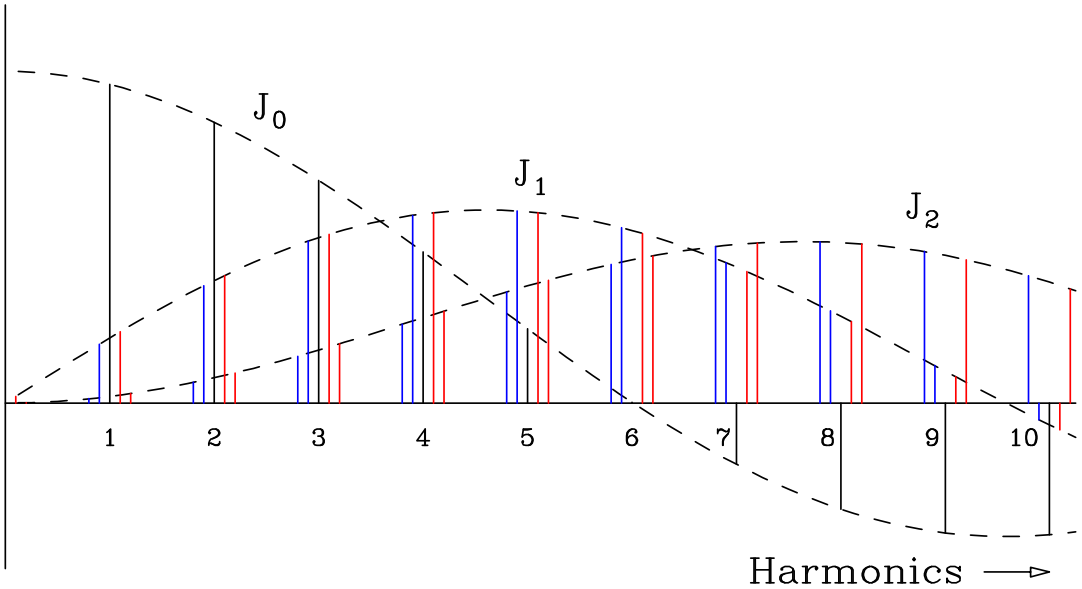

Figure 7.2: (color) Spectrum of a beam particle with synchrotron motion. Only the positive frequency is shown. The revolution harmonics ($m = 0$) are bounded by Bessel function of order zero, the first synchrotron sidebands ($m = 1$) are bounded by Bessel function of order one, and the second synchrotron sidebands ($m = 2$) are bounded by Bessel function of order two.

It is important to point out that the Bessel functions have nothing to do with the linear distribution of the bunch and here we are dealing with only a point bunch. The Bessel functions just reflect the synchrotron motion of the point bunch. If we wish to know the signal from a bunch of particles, we need to multiply Eq. (7.6) by the particle distribution $f(\varphi, \hat{\tau})$ in the synchrotron phase φ and the synchrotron oscillation amplitude $\hat{\tau}$ and integrate over φ and $\hat{\tau}$. For example, if $f(\varphi, \hat{\tau})$ is random in φ, the integral vanishes for all azimuthals except for $m = 0$, or just the revolution harmonics. This is understandable because the bunch is smooth azimuthally. The distribution must be nonuniform in the synchrotron phase before some azimuthal sidebands can be excited. We also see that the sidebands have zero width if they are excited, even if we are gathering signals from an ensemble of particles. The sidebands will be broadened, however, when the beam particles see the coupling impedance of the vacuum chamber.

Of course, to describe a bunch completely, there will also be radial modes, where the bunch oscillates with nodes at certain radii r. Let us concentrate on only one radial mode per azimuthal, the one that is most easily excited. At zero beam intensity, these modes are separated by the synchrotron frequency $\omega_s/(2\pi)$; for example, the mth mode

exhibits as a sideband $m\omega_s/(2\pi)$ away from a revolution harmonic line. This implies that at low intensities, the azimuthal modes are good eigenmodes. The radial eigenmodes, however, depend on the radial distribution of the unperturbed bunch. If the intensity of the bunch is increased, the spacings of the sidebands will change.

Here, we wish to study the collective motion of the bunch, implying that it will oscillate with a coherent frequency $\Omega/(2\pi)$. The time dependent part is written as

$$\sum_{p=-\infty}^{\infty} F_p e^{-i(p\omega_0+\Omega)t} \ , \tag{7.7}$$

where F_p is some factor depending on p and $\omega_0/(2\pi)$ is the revolution frequency. Suppose that the synchrotron dipole mode is excited, we will have $\Omega \approx +\omega_s$, provided that the intensity of the bunch is not too large. Therefore, the spectrum of the bunch will consist of only *upper* synchrotron sidebands at a distance ω_s above the harmonic lines, as shown in the top plot of Fig. 7.3. Of course, not all the sidebands will be excited equally. The excitation will depend on the driving impedance and also the bunch shape. All these are grouped into the factor F_p. However, in an oscilloscope or network analyzer, we can see only *positive* frequencies. This is equivalent to folding the spectrum about the zero frequency point, the upper synchrotron sidebands corresponding to the negative harmonics will appear as lower synchrotron sidebands for the positive frequencies, or the lower plot of Fig. 7.3. When the driving impedance is a narrow resonance, we may have $\Omega \approx -\omega_s$ instead. Suppose the narrow resonance is at frequency $\omega_r = p\omega_0 - \omega_s$ with $p > 0$. Since $\mathcal{R}e\, Z_0^{\|}(\omega)$ is symmetric about $\omega = 0$, this narrow resonance is also driving the negative frequency $-\omega_r = p'\omega_0 + \omega_s$ where $p' = -p$, which is the upper sideband of a negative harmonic. In other words, because of the definite symmetries of $\mathcal{R}e\, Z_0^{\|}(\omega)$ and $\mathcal{I}m\, Z_0^{\|}(\omega)$ and also the spectrum of synchrotron motion in Eq. (7.6) about $\omega = 0$, it is possible for us to study only the half the sidebands, either the upper ($\Omega \approx \omega_s$) or ($\Omega \approx -\omega_s$) lower. Studying the upper sidebands alone will yield exactly the same results as studying the lower sidebands alone. For this reason, we can assume all the excited synchrotron sidebands to be only upper sidebands in the language of having both positive and negative frequencies. This analysis, however, is not correct for transverse collective motion, because the synchrotron sidebands are around the tune lines which are not symmetric about the zero-frequency point.

We would like to emphasize here that the spectrum of beam particles performing synchrotron motion is very different from the spectrum of the coherent motion of beam particles. In the former, Eq. (7.6), we see all the possible modes. However, in the latter,

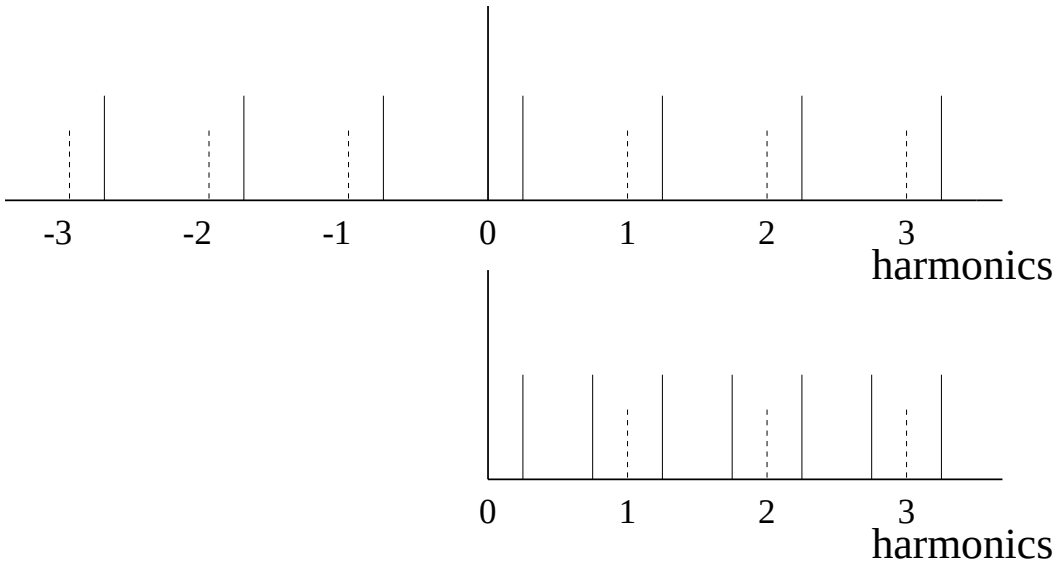

Figure 7.3: Top plot shows the synchrotron lines for both positive and negative revolution harmonics. The revolution harmonics are shown in dashes and the synchrotron *upper* sidebands in solid. Lower plot shows the negative-harmonic side folded onto the positive-harmonic side. We see upper and lower sideband for each harmonic line.

only some of those modes are excited coherently. We are looking at the coherent modes one at a time, because usually we have interest only in the one that has the fastest growth rate.

7.2 Mode Mixing

Assume a broadband impedance resonating at ω_r. The impedance will be inductive when $\omega < \omega_r$ and capacitive when $\omega > \omega_r$. If the rms length of the bunch $\sigma_\tau > \omega_r^{-1}$, the bunch particles are seeing mostly the inductive part of the impedance. We can assume that the accelerator ring is operated above the transition energy because the electrons, having small masses, are traveling at almost the velocity of light. This inductive force is repulsive opposing the focusing force of the rf voltage, thus lengthening the bunch and lowering the synchrotron frequency. Therefore, all azimuthal modes will be shifted downward, except for the dipole mode $m = 1$ at least when the beam intensity is low. The $m = 1$ does not shift because this is a rigid dipole motion and the inductive force acting on a beam particle is proportional to the gradient of the linear density as is

demonstrated in Sec. 3.2. The centroid of the bunch does not see any linear density gradient and is therefore not affected by the inductive impedance. This is very similar to the space charge self-field force. In fact, the inductive impedance is just the negative of a capacitive impedance. When the bunch intensity is large enough, the $m = 2$ mode will collide with the $m = 1$ mode, and an instability will occur if the frequencies corresponding to these two modes fall inside the resonant peak of $\mathcal{R}e\, Z_0^{\|}$. Mathematically, the frequency shifts of the two modes become complex. Since one solution is the complex conjugate of the other, one mode is damped while the other one grows. This is called *longitudinal mode-mixing* instability. Sometimes it is also known as *mode-coupling* or *mode-colliding* instability. An illustration is shown in Fig. 7.4 for a parabolic bunch of full length τ_L interacting with a broadband impedance resonating with impedance R at frequency $\omega_r/(2\pi)$.

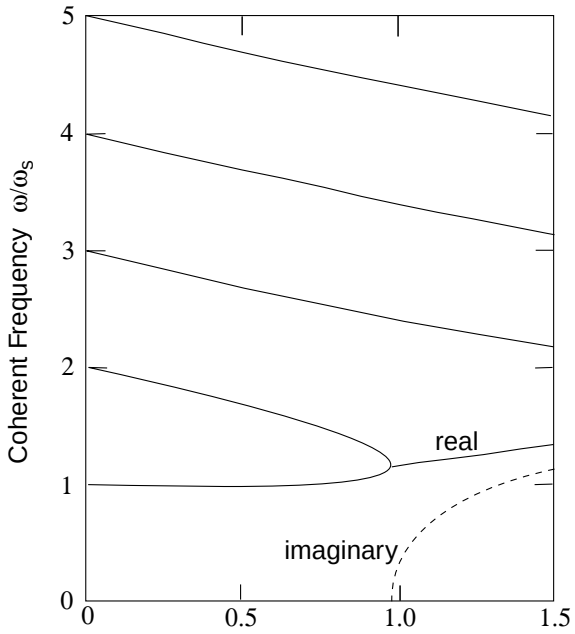

Figure 7.4: Plot showing longitudinal mode-mixing instability of a parabolic bunch of full length τ_L interacting with a broadband impedance resonating with impedance R at frequency $\omega_r/(2\pi)$. The bunch length τ_L is much longer than ω_r^{-1} so that the bunch particles are seeing the inductive part of the impedance. Thus, all modes, except for $m = 1$, shift downward.

A more thorough derivation will be given later after we study Sacherer's integral of instabilities in later chapters. Here, we just give a rough estimate of the threshold and discuss some points of interest. Just as a space charge impedance will counteract the rf focusing force below transition, here an inductive impedance will counteract the rf focusing force above transition. According to Eq. (3.58), the extra voltage seen per turn by an electron at an arrival advance τ from the effect of the inductive impedance is

$$V_{\rm ind} = \frac{3eN}{2\omega_0\hat{\tau}^2}\left|\frac{Z_0^{\|}}{n}\right|_{\rm ind}\frac{\tau}{\hat{\tau}}\ , \tag{7.8}$$

where a parabolic linear distribution for the electron bunch of half length $\hat{\tau}$ has been assumed and N is the number of particles in the bunch. Although a parabolic distribution for electron bunches is not realistic, it does provide a linear potential and ease the mathematics. The synchrotron frequency is proportional to the square root of the potential gradient, $dV_{\rm ind}/d\phi$, where ϕ is the rf phase. This extra voltage will shift the incoherent synchrotron tune downward. If the beam intensity is low, the shift can be obtained by perturbation, giving

$$\frac{\Delta\nu_s}{\nu_{s0}} = \frac{1}{2}\frac{dV_{\rm ind}/d\phi}{dV_{\rm rf}/d\phi} = \frac{3e^2N\eta}{8\pi\omega_{s0}^2\hat{\tau}^3\beta^2E_0}\left|\frac{Z_0^{\|}}{n}\right|_{\rm ind}\ . \tag{7.9}$$

All the azimuthal modes will have their frequencies shifted downward coherently by roughly by this amount also except for the $m = 1$ mode. The threshold can therefore be estimated roughly by equating the shift to the synchrotron tune. Because this shift is now large, the perturbative result of Eq. (7.9) cannot apply. Instead we equate the gradient of the extra voltage from the inductive impedance directly to the gradient of the rf voltage, to get the threshold

$$\frac{3e^2N|\eta|}{4\pi\omega_{s0}^2\hat{\tau}^3\beta^2E_0}\left|\frac{Z_0^{\|}}{n}\right|_{\rm ind} \lesssim 1\ . \tag{7.10}$$

For a broadband impedance of quality factor $Q \approx 1$,

$$\left|\frac{Z_0^{\|}}{n}\right|_{\rm ind} \approx \frac{R_s}{n_r}\ , \tag{7.11}$$

where R_s is the shunt impedance at the resonance angular frequency $\omega_r = n_r\omega_0$. Written in terms of the dimensionless current parameter ϵ in Fig. 7.4, the threshold of Eq. (7.10) translates to

$$\frac{4\pi^2eI_b|\eta|R_s}{3E_0\omega_s^2\tau_L^3\omega_r} \lesssim \frac{\pi^2}{9}\ , \tag{7.12}$$

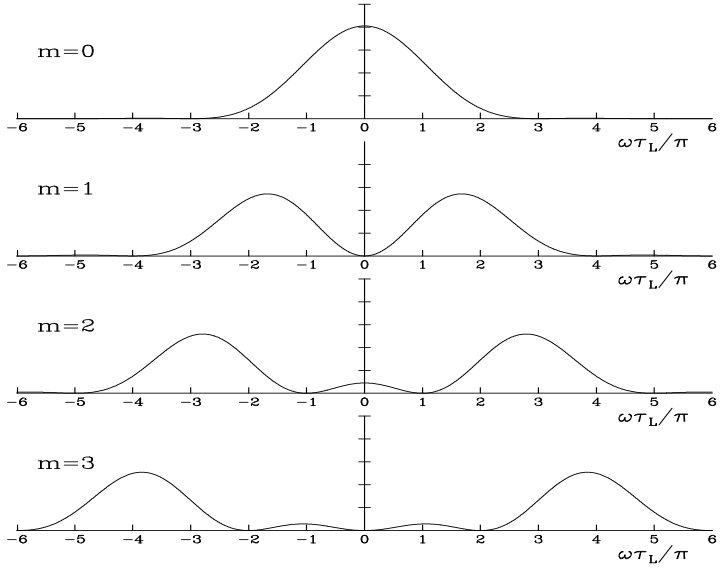

Figure 7.5: Power spectra $h_m(\omega)$ for modes $m = 0$ to 3 with zero chromaticity.

which agrees with the point of mixing in the figure very well, where $\tau_L = 2\hat{\tau}$ is the full bunch length. It can also be written as

$$\frac{R_s}{n_r} \lesssim \frac{8|\eta|E_0}{9eI_{\rm pk}\beta^2}\left(\frac{\Delta E}{E_0}\right)^2_{\rm FWHM} . \tag{7.13}$$

This is almost identical to the Keil-Schnell criterion in Eq. (6.22) with the average current replaced by the peak current. For this reason, this longitudinal mode-mixing threshold is often also referred to as the Keil-Schnell threshold. In fact, as will be shown later, unlike the Keil-Schnell criterion, the left-side of Eq. (7.13) is not the usual $|Z_0^{\parallel}/n|$ of a broad resonance. Instead it should be replaced by the *effective impedance*

$$\left|\frac{Z_0^{\parallel}}{n}\right| \longrightarrow \left.\frac{Z_0^{\parallel}}{n}\right|_{\rm eff} = \frac{\displaystyle\int d\omega \frac{Z_0^{\parallel}(\omega)}{\omega}\omega_0 h_m(\omega)}{\displaystyle\int d\omega h_m(\omega)} , \tag{7.14}$$

where $h_m(\omega)$ is the power spectrum of the mth azimuthal mode depicted in Fig. 7.1. In fact, when made dimensionless, h_m is a function of $\omega\hat{\tau}$ only. For Sacherer's approximate sinusoidal modes, the power spectra of some lower azimuthal modes are shown in Fig. 7.5. It is important to point out that it is the reactive part of the impedance that shifts the frequencies of the different azimuthal modes and the resistive part of the impedance that

drive the stability. According to Fig. 7.5, for the azimuth $m = 1$ to mix with azimuth $m = 2$, the peak of the resonance must have frequency between the peak of the power spectra of the two modes, or

$$\omega_r \sim \frac{2\pi}{\tau_L} \ . \tag{7.15}$$

In fact, this is expected, because with one or two oscillations in the linear density of the bunch, the wavelength of this instability must therefore have wavelength comparable to or shorter than the bunch length. The signal measured should correspond roughly to the rms frequency of the bunch spectrum, which is also in the microwave region because an electron bunch is often shorter than the transverse size of the vacuum chamber. For this reason, this instability is also referred to as microwave instability in the electron communities.

7.3 Bunch Lengthening and Scaling Law

In Fig. (7.4), the dashed curve denotes the growth rate of the instability. It is evident that the growth rate increases very rapidly as soon as the threshold is exceeded. We see that even when the bunch current exceeds the threshold by 20%, the growth rate reaches $\tau^{-1} \sim \omega_s$, or the growth time is $T_s/(2\pi)$, much shorter than a synchrotron period. This means that the radiation damping effect and the use of conventional feedback systems may not effective in damping the instability.

One way to avoid instability is to push the threshold to a higher value. For example, if the bunch is short enough so that $\sigma_\tau < \omega_r^{-1}$, the bunch particles will sample mostly the capacitive part of the broadband impedance. The frequencies of the azimuthal modes will shift upward instead. But the real part of the impedance will eventually bend the mode downward. However, it will become harder for the $m = 2$ and $m = 1$ modes to collide, the threshold will be relatively higher.

In reality, this instability is not devastating. The growth rate shown in Fig. (7.4) only applies when the bunch length and energy spread of the bunch are kept unchanged. As soon as the threshold is past, the bunch will be lengthened and the energy spread increased to such an extent that stability is regained again. Unlike proton bunches no overshoot is observed in electron bunches, probably because of the radiation damping. Typical plots of the bunch length and energy spread are shown in Fig. 7.6. Note that because of the balancing of synchrotron radiation and random quantum excitation, there

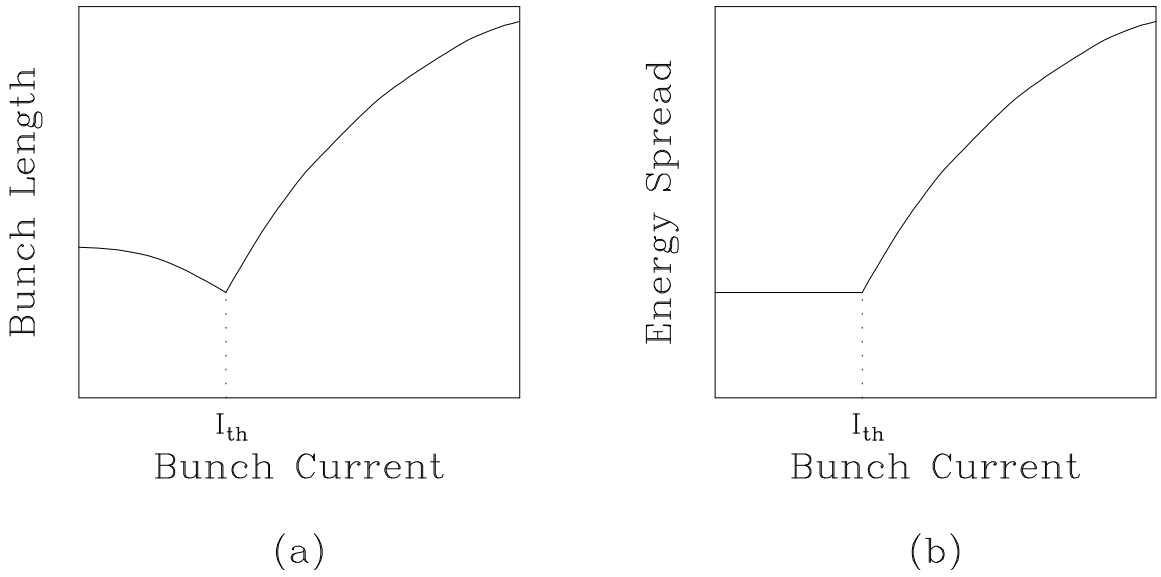

Figure 7.6: Both the bunch length and energy spread begin to grow after the bunch current exceeds its microwave instability threshold $I_{\rm th}$. (a) The bunch length starts with its natural value at zero current and becomes shortened due to the capacitive potential-well distortion, if the natural bunch length is short enough so that the capacitive part of the impedance is sampled. (b) Below the instability threshold, the energy spread is always at its natural value unaffected by the effect of potential-well distortion.

is a *natural* momentum spread σ_{δ_0} and the corresponding natural bunch length σ_{τ_0} is determined by the rf voltage. This is what we see below the threshold. For a short bunch with $\sigma_{\delta 0} < \omega_r^{-1}$, we will see the bunch length decreases as the bunch intensity increases, because the bunch samples the *attractive* capacitive impedance. This is called *potential-well distortion* which has been discussed in Chapter 3. However, the momentum spread is still determined by its natural value and is not changed. Unlike a proton bunch which can often be lost after the microwave instability threshold, the electron bunch can stabilize itself by self-increasing its length and energy spread, as illustrated in Fig. 7.6.

One way to observe this instability is to measure the increase in bunch length. We can also monitor the synchrotron sidebands and see the $m = 2$ sideband move towards the $m = 1$ sideband. This frequency shift, which is a coherent shift, as a function of beam intensity is a measure of the reactive impedance of the ring. An accurate measurement of the frequency shift of the $m = 2$ mode may sometimes be difficult. An alternate and more accurate determination of the frequency shift can be made by monitoring the

phase shift in the beam transfer function to be discussed in Chapter 14.

Noting that the mode-coupling threshold, Eq. (7.10) or Eq. (7.12), depends on only one parameter

$$\xi = \frac{\eta I_b}{\nu_s^2 E_0} \ , \tag{7.16}$$

there is a scaling law relating the bunch lengthening and the frequency dependency of the impedance sampled by the bunch. It says that the rms bunch length σ_τ above threshold is given by

$$\sigma_\tau \propto \xi^{1/(2+a)} \tag{7.17}$$

when the part of the impedance sampled by the bunch behaves like

$$Z_0^{\|} \propto \omega^a \ . \tag{7.18}$$

Here, I_b is the average beam current of the bunch. This scaling law was first derived by Chao and Gareyte [2] and has been verified experimentally in the storage ring SPEAR at SLAC. The results are plotted in Fig. 7.7. The scaling law can be proved easily by dimension argument. To proceed, substitute the effective impedance of Eq. (7.14) into the threshold condition of Eq. (7.12), and note that the power spectrum $h(\omega)$ can be made dimensionless and therefore depends on $\omega\sigma_\tau$ only (Exercise 7.3). A similar proof will be given later in Sec. 13.3 below. Note that if the Keil-Schnell criterion is applied, we always have $\sigma_\tau \propto \xi^{1/3}$ or $a = 1$, implying a long bunch seeing the inductive part of the impedance. However, for SPEAR, measurements point to $\sigma_\tau \propto \xi^{0.76}$ or $a = -0.68$, implying that the SPEAR bunch is short enough to sample the capacitive part of the impedance. This clearly demonstrates that the Keil-Schnell criterion is only suitable for long bunches which sample the inductive part of the broadband impedance, and cannot be used in an electron machine where the bunch length is so short that the capacitive part of the impedance is sampled. There is another big difference between the microwave instability for coasting beam and the mode-mixing instability discussed here. Above transition, which is true for nearly all electron rings, the tear-drop stability curve of the coasting-beam based theory states that the beam will be unstable if it is driven by a capacitive impedance which is large enough. However, it can be shown that pure reactive impedance cannot lead to mode-mixing instability. The modes may cross each other when the frequency shifts are large enough, but no instability will materialize. (See Exercise 13.3 below.)

This instability is not a devastating instability, because it results only in the blowup of the bunch area. In fact, many storage rings, especially collider rings, operate above

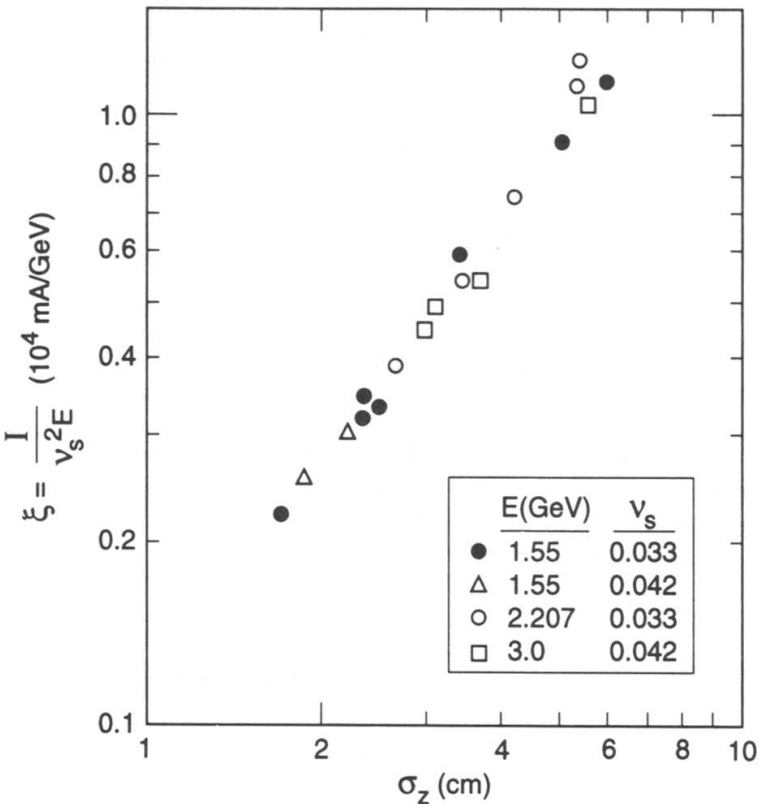

Figure 7.7: RMS bunch length σ_Z versus the scaling parameter ξ for the electron storage ring SPEAR. The momentum compaction factor has been kept constant. The measurement results indicate that $\sigma_\tau \propto \xi^{1/(2+a)}$ with $a = -0.68$.

this threshold, because a much higher beam intensity and therefore luminosity can be attained. However, this may not be the situation for a light source, where we always want to have shorter bunches so as to have smaller spot sizes for the synchrotron light. In order to accomplish this, the electron ring must be carefully designed so that the impedance is as small as possible. On the other hand, it is very difficult to reduce the impedance in a ring already built. For example, some capacitive structures had been placed in the SLAC damping rings, so as to reduce the inductive impedance of the rings. The threshold of the mixing of the $m = 2$ and $m = 1$ mode has been actually pushed higher. However, the beam particles are now seeing mostly the real part of the impedance, which distorts the bunch asymmetrically bringing out the importance of other radial excitation modes. These radial modes actually collide at a threshold much lower than the previous threshold before the modification. Fortunately, this instability due to the mixing of radial modes is much weaker than the instability due to the mixing

of azimuthal modes [4].

7.4 Sawtooth Instability

Before the modification of the vacuum chambers in the SLAC Linear Collider (SLC) damping rings, a new form of longitudinal instability coupling with synchrotron radiation damping was observed. Upon the injection of a bunch, the bunch length decreased rapidly with a longitudinal damping time of the order of 2 ms. When the bunch length passed below a threshold, a sudden blowup in bunch length occurred in a time span comparable to or shorter than the 10 μs synchrotron period, as illustrated in Fig. 7.8. This process was self-limiting because of the nonlinear nature of the short-range wake fields responsible for blowing up the bunch. Since the blowup is faster than a synchrotron period, this might have been the type of coasting-beam based microwave instability governed by the Boussard-modified Keil-Schnell criterion. Once the blowup ceased, the bunch damped down until the threshold was reached again in about a synchrotron damping time of $\sim$ 1.3 ms. Thus, a cyclical repetition of the instability was observed and termed according to its shape *sawtooth instability* [5].

The time-dependent nature was seen in the bunch-length signal from the beam-position-monitor (BPM) electrodes and the bunch-phase signal from the synchronous-phase monitor. The bunch phase can be referenced to either the 714 MHz rf of the damping ring or to the 2856 MHz S-band rf of the linac. The synchronous beam phase angle is given by $\phi_s = \sin^{-1}(U_s/V_{\rm rf})$, where U_s is the energy loss per turn as a result of synchrotron radiation. The higher-order mode losses of a bunch are functions of the line charge density and are inversely proportional to the bunch length. As the bunch blew up, the higher-order losses decreased and the beam phase shifted by about 0.5° at 714 MHz during a sawtooth. This translated into a 2° jump at the S-band in the linac. This magnitude of phase error caused a problem with the rf bunch-length compressor in the ring-to-linac beam line. When this instability took place, the bunch would be incorrectly launched into the linac and might eventually be lost on the downstream collimators, causing the linac to trip the machine protection circuits. For some consequences, see Exercises 7.4 and 7.5.

There is a threshold for this instability, which occurred at around 3×10^{10} particles per bunch for a nominal rf voltage of 1 MV. At higher intensity, the sawteeth appeared

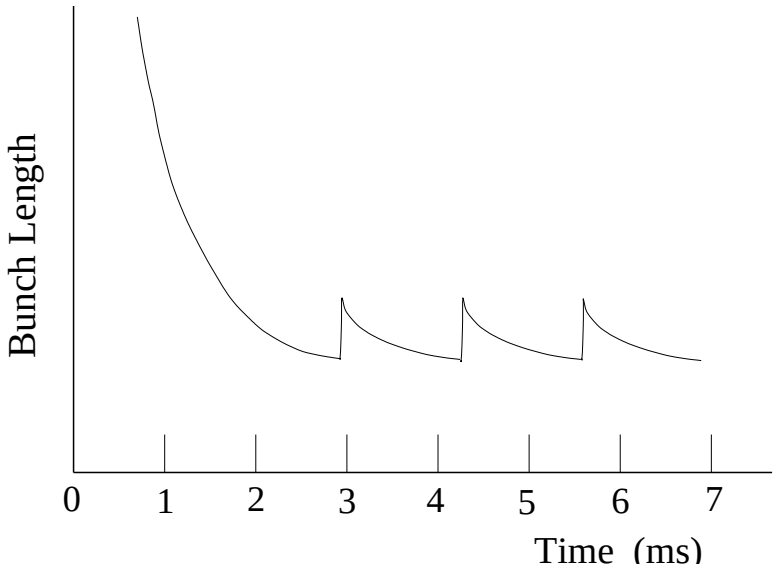

Figure 7.8: Plot of bunch length versus time at the injection of the SLAC Damping ring with an intensity of 3×10^{10} particles per bunch. The bunchlength was damped rapidly in the first 2 ms after injection to a point where it was unstable against microwave instability. Rapid growth took place until the bunch was self-stabilized. After that it was damped by synchrotron radiation to below the instability threshold. This repetition has the shape of sawteeth.

closer together in time. The process could be viewed as a relaxation oscillator where the period is a function of the bunch-length damping time and the trigger threshold. The damping time is constant but the bunch length at which the bunch went unstable increased at higher intensities. When the bunch intensity was increased to 4×10^{10} particles, a transition occurred to a second regime with "continuous sawteeth".

With the installation of new SLC damping-ring vacuum chambers, the sawtooth instability did not go away as it was expected by simulations. On the contrary, the threshold went down from 3×10^{10} to 1.5-2×10^{10} particles per bunch. The new instability has a similar behavior, but it apparently is very much milder and does not affect the phase mismatch of the linac downstream as severely as the old instability. An intense investigation has been going on to study this instability even after the installation of the new vacuum chambers. Podobedov and Siemann [6] tried to measure the longitudinal density bunch profiles from the synchrotron light with a high-resolution Hamamatsu streak camera during the instability. The phase of oscillation of the bunch density was obtained from the high-frequency BPM signals, processed and digitized by an oscillo-

scope. The 295 chosen profiles were binned according to their phases. The $+\frac{\pi}{2} \pm \frac{\pi}{4}$ phase bin implies near maximum deviation, while the $-\frac{\pi}{2} \pm \frac{\pi}{4}$ phase bin implies near minimum deviation. The average shapes for the two phase bins and the overall average profile are shown in Fig. 7.9. The wavelength of oscillation is about 30 ps. The oscillating part of

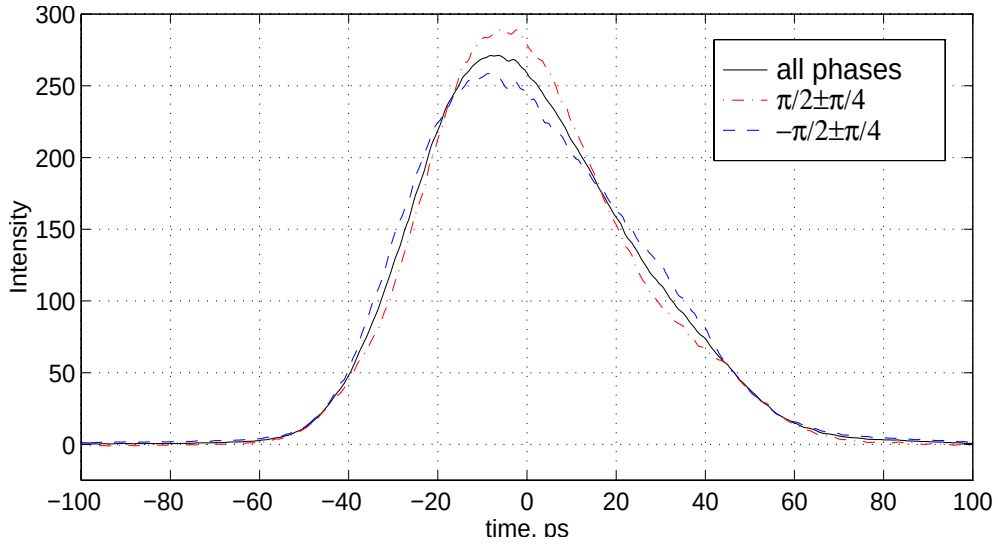

Figure 7.9: (color) Beam density profiles during an instability burst captured by streak camera. The average is in solid. Those with the phase $+\frac{\pi}{2} \pm \frac{\pi}{4}$ are in red dot-dashes and those with phase $-\frac{\pi}{2} \pm \frac{\pi}{4}$ are in blue dashes.

the density was next filtered out using

$$\delta\rho(\tau) = \left\langle \frac{\rho_k(\tau) - \rho_0(\tau)}{\sin\phi_k} \right\rangle \ , \tag{7.19}$$

where ρ_k are all the profiles with the phases ϕ_k ($k = 1,\ 2,\ \cdots,\ 295$), ρ_0 is the phase-averaged profile, and the angle brackets denote the median value. The structure obtained is shown in Fig. 7.10. This linear density resembles the $m = 2$ quadrupole mode in Fig 7.1 with the stationary distribution subtracted. The structure in the longitudinal phase space is shown in the corner of the figure. The ratio of the positive peak area to the one under ρ_0 is about 3%, which measures the amount of redistributed particles creating the quadrupole structure.

The instability was further pursued in the frequency domain by Podobedov and Siemann [7]. A bunch containing 3.5×10^{10} positrons was scanned in the SLC positron damping ring for the whole store of several minutes, during which the bunch intensity

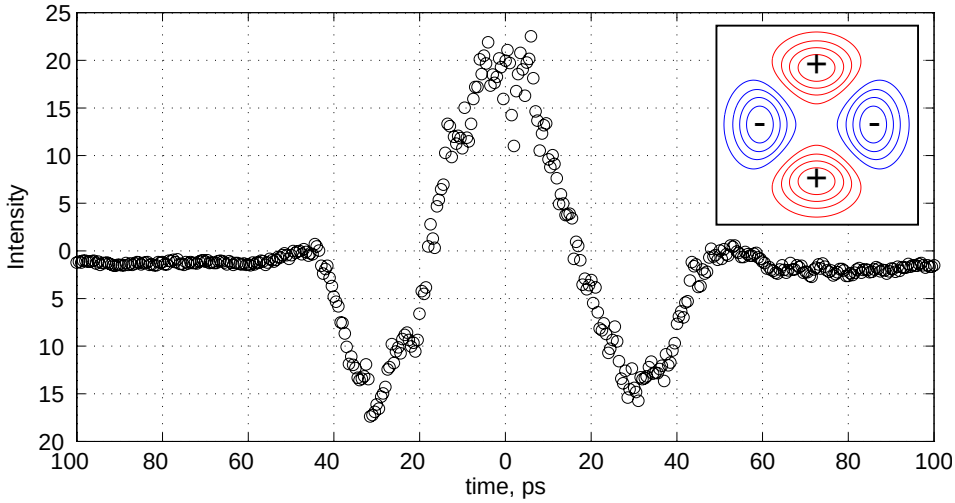

Figure 7.10: (color) Bunch density oscillation with the average distribution subtracted. The structure resembles the projection of the azimuthal $m = 2$ oscillation.

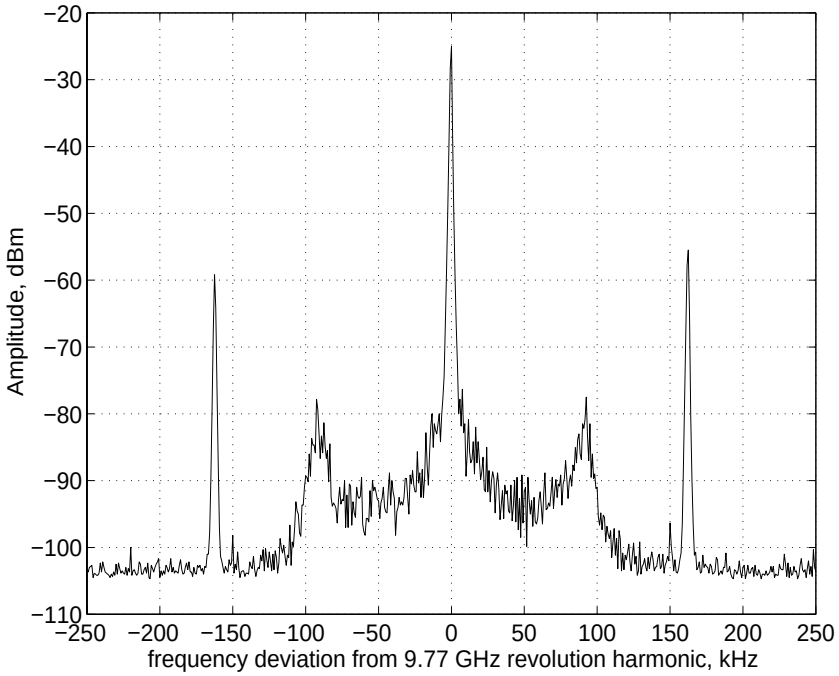

Figure 7.11: Typical spectrum at 3×10^{10} ppb around the 1149th revolution harmonic (9.77 GHz) in the SLC positron damping ring after the installation of the new vacuum chamber. The quadrupole mode sidebands are excited and are displaced $\sim$ 160 kHz from the harmonic, about 10% less than twice the zero-current synchrotron frequency at 690 kV rf.

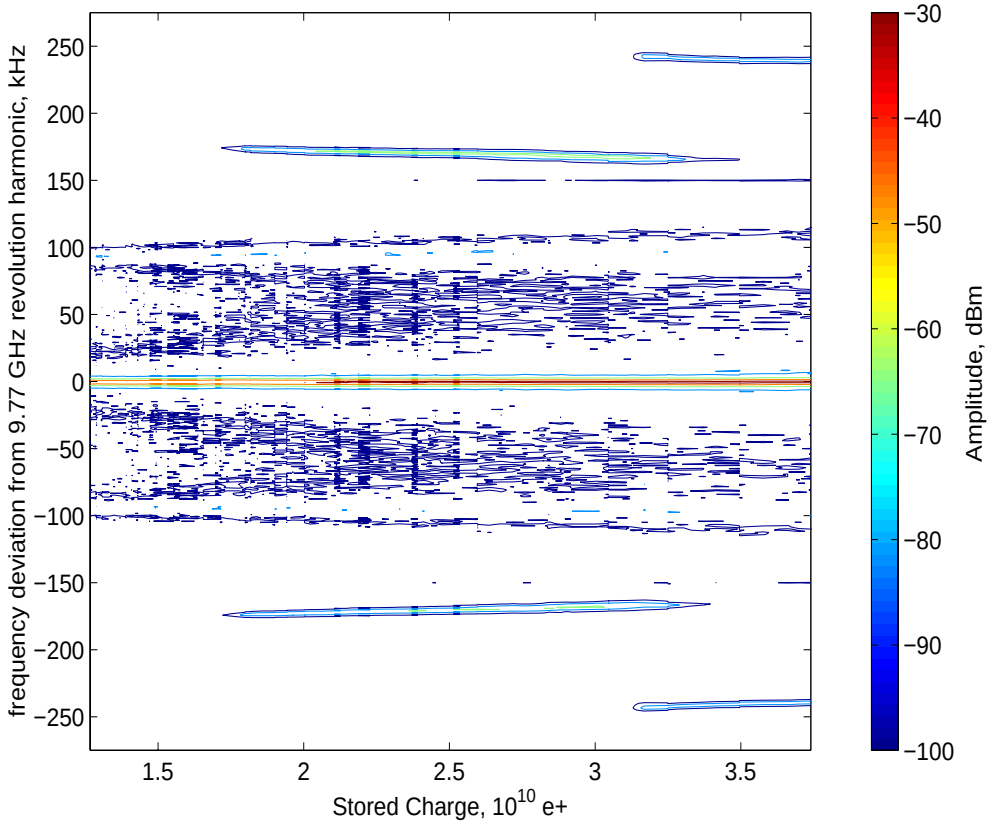

Figure 7.12: (color) Contour plot of all the spectrum analyzer sweeps for a store of a positron bunch in the SLC damping ring. The bunch intensity decays from 3.5×10^{10} to almost half near the end of the store. Sextupole mode instability is first seen and switches to quadrupole mode instability around 3.2-3.4 $\times 10^{10}$ ppb. All instabilities stop below the intensity of 1.7×10^{10} ppb.

decayed by roughly a factor of two. The signal processing system consists of a square-law detector which demodulates the instability signal from the sidebands to high-frequency revolution harmonics. This signal is subsequently amplified and the higher-order mixing products are removed by a low-pass filter. Figure 7.11 shows a typical spectrum at bunch intensity 3×10^{10} around the 1149th revolution harmonic (9.77 GHz). We see the quadrupole mode of instability and the quadrupole sidebands to the harmonic displaced by about 160 kHz. This is roughly 10% lower than twice the zero-current synchrotron frequency at the rf voltage of 690 kV. The contour plot in Fig. 7.12 shows all the spectrum analyzer sweeps for the whole store. One can see how the instability jumps from sextupole to a quadrupole mode around the intensity of 3.2-3.4 $\times 10^{10}$ ppb. The

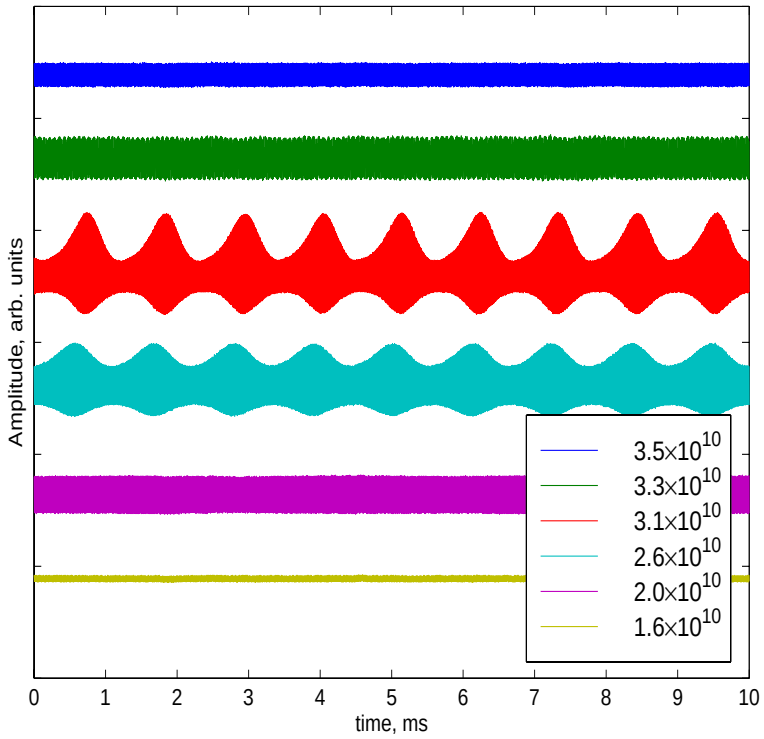

Figure 7.13: (color) Oscilloscope traces of the instability signal from different values of the stored positron bunch. Sawtooth behaviors occur near the intensity of 2.6-3.1 $\times$ 10^{10} ppb when the mode of excitation is purely quadrupole.

quadrupole mode threshold is about 1.7×10^{10} ppb with its frequency linearly decreasing at a rate of $\sim$ 5 kHz/10^{10} ppb. Such a behavior is usually attributed to the inductive portion of the ring impedance. However, we do not see the crossing of the quadrupole and sextupole modes or the crossing of the quadrupole and dipole modes. This indicates that the instabilities may arise from the mixing of radial modes belonging to one azimuthal, as postulated by Chao [8]. We believe that before the modification of the vacuum chamber, the instability, which was very much strong, did arise from the mixing of two azimuthal modes. In any case, the physics behind the sawtooth instability is still far from understood.

Along with the spectrum analyzer data, Fig. 7.13 shows some oscilloscope traces taken concurrently. The top trace at 3.5×10^{10} ppb corresponds to a constant amplitude sextupole mode. The next trace corresponds to the case when both sextupole and quadrupole modes coexist. At even smaller current, 2.6-3.1 $\times$ 10^{10} ppb, the two traces

in the middle show the sawtooth bursting behavior of the instability and correspond to pure quadrupole mode. Finally below 2.5×10^{10} ppb, the bursts disappear and the quadrupole mode oscillates with constant amplitude.

Lowering the rf voltage is a means of increasing the equilibrium bunch length and extending the intensity threshold. This is because the Landau damping from the energy spread, which is determined by synchrotron radiation, is unchanged, but lengthening the bunch reduces the local peak current and brings the bunch below the Keil-Schnell threshold according to Eq. (6.22). A low rf voltage, however, is not suitable for efficient injection and extraction for the damping rings. Before the installation of the new vacuum chamber into the damping rings, the rf voltage was ramped down from 1 MV to 0.25 MV approximately 1 ms after injection, as illustrated in Fig. 7.14. It was ramped up back to 1 MV 0.5 ms before extraction. In this way the onset of sawtooth instability had been suppressed up to an intensity of 3.5×10^{10} per bunch.

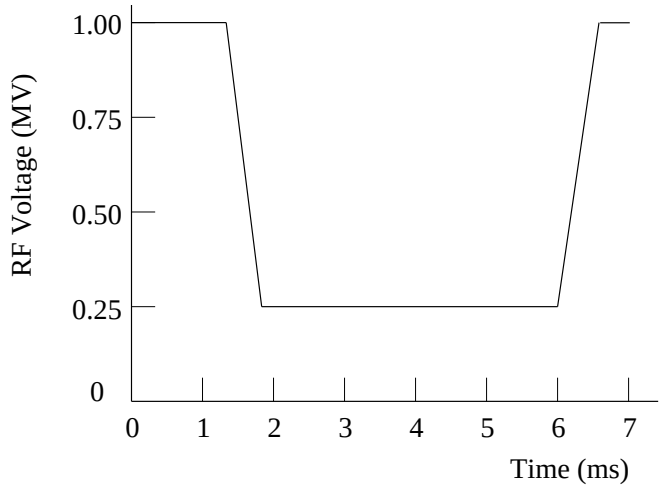

Figure 7.14: The rf voltage was lowered in the SLAC damping ring after injection and before extraction, thus lengthening the bunch and reducing the local charge density. This raised the microwave instability threshold and prevented the sawtooth instability.

Here, we want to mention another difference between electron and proton bunches. Although lowering the rf voltage may stabilize an electron bunch, this certainly will not work for a proton bunch. This is because for an electron bunch, the energy spread is determined by synchrotron radiation and will not change as the rf voltage is lowered. On the other hand, for a proton bunch, the bunch area conserves. Thus, lowering the rf voltage will diminish the energy spread instead, although the local linear density is

decreased. Recall the Boussard-modified Keil-Schnell criterion [3] or the Krinsky-Wang criterion [1] for Gaussian energy spread distribution,

$$\left|\frac{Z_0^{\|}}{n}\right| < \frac{2\pi|\eta|E_0}{eI_{\rm pk}\beta^2}\left(\frac{\sigma_{_E}}{E_0}\right)^2 \ . \tag{7.20}$$

Assuming also a Gaussian linear distribution,

$$I_{\rm pk} = \frac{eN}{\sqrt{2\pi}\sigma_\tau} \ , \tag{7.21}$$

where σ_τ is the rms bunch length in time. Constant bunch area of a proton bunch implies constant $\sigma_\tau\sigma_{_E}$. Thus, the threshold is directly proportional to the energy spread $\sigma_{_E}$ and is inversely proportional to the bunch length σ_τ. Reducing the rf voltage will make the proton bunch more susceptible to microwave instability. Such instability is very often seen when an rf rotation is perform to obtain a narrow proton bunch. The rf voltage is first lowered adiabatically in order to lengthen the bunch to as long as possible. The rf voltage is then raised suddenly to its highest possible value. The long and small-energy-spread bunch will rotate after a quarter of a synchrotron oscillation to a narrow bunch with large energy spread. Because it takes a lot of time to reduce the rf voltage adiabatically, the beam will often suffer from microwave instability when the momentum spread is small. To avoid this instability, one way is to snap the rf voltage down suddenly so that the rf bucket changes from Fig. 7.15(a) to 7.15(b). The bunch will be lengthened after a quarter synchrotron oscillation. The rf voltage is then snapped up again as in Fig. 7.15(c) so that the lengthened bunch rotates into a narrow bunch as required. Since snapping the rf voltage is much faster than lowering it adiabatically, this may prevent the evolution of microwave instability. Such a method is also used in bunch coalescence at Fermilab.

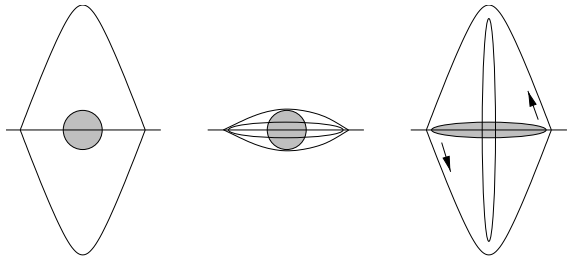

Figure 7.15: Bunch shortening is performed by snapping down the rf voltage $V_{\rm rf}$, rotating for $\frac{1}{4}$ synchrotron oscillation, snapping up $V_{\rm rf}$, and rotating for another $\frac{1}{4}$ synchrotron oscillation.

7.5 Exercises

7.1. Derive the incoherent synchrotron tune shift in Eq. (7.9) driven by an inductive impedance.

7.2. (1) Derive the mode-mixing threshold, Eq. (7.10), by equating the synchrotron tune shift to the synchrotron mode separation.
(2) Rearrange the result to obtain the Keil-Schnell like criterion of Eq. (7.13).

7.3. Prove the scaling law about bunch length dependency using dimension argument as outlined in the text.

7.4. There is a difference in energy loss between the head and tail of a bunch in a linac because of the longitudinal wake. Take the SLAC linac as an example. It has a total length of $L = 3$ km and rf cavity cell period $L_0 = 3.5$ cm. The bunch consists of $N = 5 \times 10^{10}$ electrons and is of rms length $\sigma_z = 1.0$ mm. The longitudinal wake per cavity period is $W_0' = 6.29$ V/pC at $z = 0^+$ mm and 4.04 V/pC at $z = 1$ mm.
(1) Consider the bunch as one macro-particle, find the total energy loss by a particle traveling through the whole linac, taking into account the fundamental theorem of beam loading (proved in Sec. 8.4.1 below) that a particle sees exactly one half of its own wake.
(2) Consider the bunch as made up of two macro-particles each containing $\frac{1}{2}N$ electrons, separated by the distance σ_z. Find the energy lost by a particle in the head and a particle in the tail as they traverse the whole linac.

7.5. A more detailed computation gives 1.2 or 2.1 GeV as the energy lost by a particle $\frac{1}{2}\sigma_z$ ahead or behind the bunch center. This energy spread needs to be corrected to ensure the success of final focusing at the interaction point of the SLAC Linear Collider. The rf voltage is 600 kV per cavity period and the rf frequency is 2.856 GHz.
(1) Explain why we cannot compensate for the energy spread by placing the tail of the bunch ($\frac{1}{2}\sigma_z$ behind bunch center) at the crest of the rf wave so that the tail can gain more energy than the head.
(2) The correct way to eliminate this energy spread is to place the center of the bunch at an rf phase angle ϕ ahead the crest of the rf wave such that the gradient of the rf voltage is equal to the gradient of the energy loss along the bunch. Show that the suitable phase is $\phi = 17.3°$.

(3) The accelerating gradient will decrease with this rf phase offset. A compromise phase is $\phi = 12°$. Compute the head-tail energy spread with this phase offset and compare the effective accelerating gradients in the two situations.
(4) Assume that the sawtooth instability adds a $\pm 2°$ uncertainty in rf phase error, implying that ϕ now becomes 10 to 14°. Compute the head-tail energy spread and the center energy uncertainty under this condition. Repeat the computation if the rf phase jitter is $\pm 5°$ instead.

7.6. A particle at time advance τ inside a bunch of linear particle distribution $\lambda(\tau)$ (normalized to total number of particles N when integrated over τ) sees a voltage due to the longitudinal wake,

$$V(z) = -e \int_{\tau}^{\infty} W_0'(z/v)\lambda(\tau - z/v)\frac{dz}{v} \tag{7.22}$$

and suffers an energy loss. The energy loss of the whole bunch, which is often called the *parasitic loss* is

$$\Delta\mathcal{E} = e^2 \int_{-\infty}^{\infty} V(\tau)\lambda(\tau)\frac{ds}{v} \ . \tag{7.23}$$

(1) Show that the parasitic loss can also be written as

$$\Delta\mathcal{E} = -2\pi e^2 \int_{-\infty}^{\infty} Z_0^{\parallel}(\omega)\left|\tilde{\lambda}(\omega)\right|^2 d\omega \ , \tag{7.24}$$

where the Fourier transform of the linear distribution is defined as

$$\lambda(\tau) = \int_{-\infty}^{\infty} \tilde{\lambda}(\omega)e^{-i\omega\tau}d\tau \ . \tag{7.25}$$

(2) Show that the space charge-like wake field $W_0'(z) = L\delta'(z/v)$ does not cause parasitic energy losses.
(3) For a Gaussian bunch with rms length σ_τ, show that the parasitic energy loss per unit length due to the resistivity of a circular beam pipe of radius b is

$$\Delta\mathcal{E} = \frac{e^2N^2\Gamma(\frac{3}{4})}{4\pi^2 b\sigma_\tau^{3/2}}\left(\frac{Z_0\mu_r}{2\sigma c}\right)^{1/2} \ , \tag{7.26}$$

where σ is the wall conductivity, μ_r is the wall relative magnetic permeability, and $\Gamma(\frac{3}{4}) = 1.22542$ is the Gamma function. You may use Eq. (1.42) for the wall impedance.

(4) For the SSC the stainless steel beam pipe radius is $b = 1.65$ cm with a conductivity of $\sigma = 2.0 \times 10^6$ $(\Omega\text{-m})^{-1}$ at cryogenic temperature and relative magnetic permeability $\mu_r \approx 1$. There are two proton beams, each of which has $M = 17280$ bunches with $N = 7.3 \times 10^9$ protons each and an rms length $\sigma_z = 7$ cm. Compute the power load on the cryogenic system due to the parasitic power heating of the beam pipe wall. To reduce the cryogenic load, the inner surface of the beam pipe is coated with a layer of copper having $\sigma = 1.8 \times 10^9$ $(\Omega\text{-m})^{-1}$ and $\mu_r = 1$ at cryogenic temperature. Recompute the heat load.

Bibliography

[1] S. Krinsky and J.M. Wang, Particle Accelerators **17**, 109 (1985).

[2] A.W. Chao and J. Gareyte, Part. Accel. **25**, 229 (1990).

[3] E. Keil and W. Schnell, CERN Report TH-RF/69-48 (1969); V.K. Neil and A.M. Sessler, Rev. Sci. Instr. **36**, 429 (1965); D. Boussard, CERN Report Lab II/RF/Int./75-2 (1975).

[4] K. Bane, etal, *High-Intensity Single Bunch Instability Behavior in the New SLC Damping Ring Vacuum Chamber*, Proc. 1995 Particle Accelerator Conference, May 1-5, 1995, Dallas, Texas, p.3109.

[5] P. Krejcik, K. Bane, P. Corredoura, F.J. Decker, J. Judkins, T. Limberg, M. Minty, R.H. Siemann, and F. Pedersen, *High Intensity Bunch Length Instabilities in the SLC Damping Ring*, Proc. 1993 Particle Accelerator Conference and International Conference on High-Energy Accelerators, Washington, DC, May 17-20, 1993, p.3240.

[6] B. Podobedev and R. Siemann, Proc. 1997 Particle Accelerator Conference, Vancouver, B.C., Canada, May 12-16, 1997, Ed. Comyn, M.K. Craddock, M. Reoser, and J. Thomson, p.1629.

[7] B. Podobedev and R. Siemann, *Signals from Microwave Unstable Beams in the SLC Damping Rings*, Proc. 1999 Particle Accelerator Conference, New York, NY, March 29 - April 2, 1999, p.146.

[8] A. Chao etal, Proc. 1995 Particle Accelerator Conference, 1995, p.3040.